Materials Research Proceedings 41 (2024) 1231-1239 https://doi.org/10.21741/9781644903131-137

Modelling ductile damage of a textured aluminum alloy based on a non-quadratic yield function

BRITO João P.[1,a], OLIVEIRA Marta C.[1,b]* and ALVES José Luís[2,c]

[1]CEMMPRE, ARISE, Department of Mechanical Engineering, University of Coimbra, Pinhal de Marrocos, 3030-788 Coimbra, Portugal

[2]Microelectromechanical Systems Research Unit, University of Minho, Campus de Azurém, 4800-058 Guimarães, Portugal

[a]joao.brito@uc.pt, [b]marta.oliveira@dem.uc.pt, [c]jlalves@dem.uminho.pt

Keywords: Ductile damage, Porosity, Homogenization, Deep drawing, Orthotropy

Abstract. The development of more sophisticated constitutive models is essential for improving the reliability of metal forming process simulations. The main objective of this work is to employ a Gurson-type [1] porous criterion to assess the ductile damage distribution of a strongly textured AA5042-H2 sheet during a single-stage cup-drawing process. The anisotropy of the dense phase is described with the non-quadratic form of the CPB06ex2 [2] criterion using two linear transformations. In line with Gurson's homogenization theory, the plastic behavior of the porous solid is described by an approximate macroscopic strain-rate potential (SRP) using the classical Rice and Tracey trial fields. The particularity of this implementation is that the macroscopic potentials are not evaluated via analytical functions, but by numerical integration of the local fields [3]. It is shown that such approach is viable from the computational standpoint and opens the door for materials with intricate plastic behavior to be modeled within the framework of porous media.

Introduction

Traditionally, constitutive models are represented by closed-form expressions for two primary reasons: first, to minimize computational costs, and second, to facilitate their integration into numerical simulation schemes such as the Finite Element Method (FEM). Regrettably, due to inherent mathematical constraints, obtaining closed-form expressions in the context of porous media may require the incorporation of one or more simplifying hypotheses, often accompanied with detrimental modelling effects (e.g. the Cauchy-Schwartz inequality), or may even be unattainable. Opportunely, recent strides in the computational power-to-cost ratio have facilitated the adoption of a fully numerical approach to constitutive modelling. Such approach, by design, circumvents the challenges associated with obtaining closed-form expressions and presently allow for numerical simulations to be conducted within reasonable computational timeframes. Based on this notion, Brito [3] recently proposed a numerical integration scheme for evaluating the stress- and strain-rate- plastic potentials for ductile porous solids containing randomly distributed spherical voids whose matrix behaviour is described by the non-quadratic orthotropic stress potential of Plunkett et al. [2]. The goal of this paper is to apply the latter formulation to evaluate the ductile damage distribution of a strongly textured AA5042-H2 sheet during a single-stage cylindrical cup-drawing process. Indeed, given its industrial significance and geometric simplicity, the cylindrical cup-drawing process stands out as one of the most frequently employed benchmarks for evaluating the performance of constitutive criteria. The manifestation of plastic anisotropy gives rise to earing phenomena, characterized by the undulation of the top edge of the fully drawn cup. The extent of texture in the material can dictate the occurrence of four, six, or more ears resulting from the drawing process. The application example adopted in this work is based on the experimental results of Yoon et al. [4], which reported a cup with eight ears. Moreover, these

authors employed the Plunkett et al. [2] criterion with two transformations (CPB06ex2) to simulate the forming process and found that the model predicted a similar earing profile. While the geometry of the completely drawn cup can be assessed with such formulation (valid for dense, plastic isochoric, materials), no conclusion can be drawn regarding the damage distribution in the component. This problem is now readdressed within the scope of porous media, for which the porosity distribution quantifies the damage state. It is shown that the numerical homogenization scheme is, indeed, feasible from the computational perspective and is a promising tool for evaluating the damage state of anisotropic ductile metals and alloys.

The general scheme of notation is as follows. Scalars and scalar-valued functions are denoted with light-face letters, e.g. $(A,b,\ldots)$; vectors with under bar italic Latin and Greek bold-face letters, e.g. $(\underline{\boldsymbol{A}},\underline{\boldsymbol{b}},\ldots)$; second-order tensors or tensor-valued functions with italic Latin and Greek bold-face letters $(\boldsymbol{A},\boldsymbol{b},\ldots)$; fourth-order tensors with calligraphic majuscules, e.g. $(\mathsf{A},\mathsf{B},...)$. The corresponding pseudo-vectorial and matrix Voigt notation are represented with upright Latin bold-face letters $(\mathbf{A},\mathbf{b},\ldots)$. The double-contracted tensor products is defined as $\boldsymbol{A}:\boldsymbol{B}=A_{ij}B_{ij}$, and $(\mathsf{C}:\boldsymbol{A})_{ij}=\mathsf{C}_{ijkl}A_{kl}$. The summation convention over repeated indices is employed.

Plasticity model

The employed macroscopic strain-rate potential results from the kinematic Hill-Mandel homogenization framework considering: (i) an hollow sphere of domain Ω, with outer radius B, containing a concentric spherical void of radius A occupying a domain ω; (ii) the (kinematically admissible) Rice and Tracey [5] velocity fields; and (iii) the microscale (alias local) plasticity model governed by the yield criterion, $f(\boldsymbol{\sigma})$, of Plunkett et al. [2], i.e.:

$$\begin{aligned} &f(\boldsymbol{\sigma},k^{(n)},\mathbf{L}^{(n)},a,\sigma_1^{\mathrm{T}}) \equiv \varphi(\boldsymbol{\sigma},k^{(n)},\mathbf{L}^{(n)},a)-\sigma_1^{\mathrm{T}}=0,\ \ n=1,...,n_{\mathrm{ex}},\\ &\varphi=m\left(F\right)^{\frac{1}{a}},\ \text{with}\ F=\sum_{n=1}^{n_{\mathrm{ex}}}F^{(n)}\ \text{and}\ F^{(n)}=\sum_{i=1}^{3}\left(\left|\hat{s}_{p_i}^{(n)}\right|-k^{(n)}\hat{s}_{p_i}^{(n)}\right)^{a}, \end{aligned} \tag{1}$$

where $n_{\mathrm{ex}}\geq 1$ is the number of orthotropic transformations, a is the the homogeneity degree, σ_1^{T} is the yield stress in uniaxial tension along the 1-direction of the orthotropy axes, $\hat{s}_{p_i}^{(n)},\ i=1,2,3,$ are the eigenvalues of the n-th transformed stress tensor, $\hat{\boldsymbol{s}}^{(n)}=\mathbf{L}^{(n)}:\boldsymbol{s},\ \mathbf{L}^{(n)}=\mathbf{C}^{(n)}:\mathbf{K}$ is the n-th fourth-order deviatoric transformation tensor, and $\mathbf{C}^{(n)}$ is a major-symmetric orthotropic tensor whose Voigt 6x6-matrix notation, $\mathrm{C}_{IJ}^{(n)}\leftarrow\mathsf{C}_{ijkl}^{(n)},\ I,J=1,...,6,\ i,j,k,l=1,2,3,$ is in the form:

$$\mathbf{C}^{(n)}=\begin{bmatrix} C_{11}^{(n)} & C_{12}^{(n)} & C_{13}^{(n)} & 0 & 0 & 0\\ C_{12}^{(n)} & C_{22}^{(n)} & C_{23}^{(n)} & 0 & 0 & 0\\ C_{13}^{(n)} & C_{23}^{(n)} & C_{33}^{(n)} & 0 & 0 & 0\\ 0 & 0 & 0 & C_{44}^{(n)} & 0 & 0\\ 0 & 0 & 0 & 0 & C_{55}^{(n)} & 0\\ 0 & 0 & 0 & 0 & 0 & C_{66}^{(n)} \end{bmatrix}, \tag{2}$$

$\mathsf{K}_{ijkl}=1/2(\delta_{ik}\delta_{jl}+\delta_{il}\delta_{jk})-1/3(\delta_{ij}\delta_{kl}),\ i,j,k,l=1,2,3,$ is the isotropic fourth-order deviatoric unit tensor and δ_{ij} is the Kronecker delta. In Eq. 1, $k^{(n)}$ is the tension-compression asymmetry parameter associated with the transformation n, and m is a material constant defined such that $\varphi(\boldsymbol{\sigma})$ reduces σ_1^{T} for uniaxial tensile loadings and it is given in terms of $\mathbf{L}^{(n)}$ and $k^{(n)}$ as:

$$m=\left(\sum_{i=1}^{n_{ex}}\bar{m}^{(n)}\right)^{-\frac{1}{a}},\ \text{with}\ \bar{m}^{(n)}=\sum_{i=1}^{3}\left(\left|\Phi_i^{(n)}\right|-k^{(n)}\Phi_i^{(n)}\right)^a, \tag{3}$$

where $\Phi_i^{(n)},\ i=1,2,3$ are the components $\mathsf{L}_{ii11}^{(n)},\ i=1,2,3$ (no sum), respectively, (or, equivalently, the non-zero components of the first column of the 6x6-matrix form representation of $\mathsf{L}^{(n)}$). Convexity is guaranteed for any integer $a\geq 1$ and for $k^{(n)}\in[-1,1]$ (for the proof refer to [6]). In Eq. 1, $\varphi(\boldsymbol{\sigma})\equiv\bar{\sigma},$ is the *stress potential* (i.e. equivalent stress measure). Under associated plasticity conditions, it is possible to show (see [3]) that it exists a dual (alias conjugated or polar reciprocate) potential of $\varphi(\boldsymbol{\sigma})\equiv\bar{\sigma},$ also convex, known as the *strain-rate potential* (SRP), $\psi(\boldsymbol{d}^{\mathrm{p}})\equiv\dot{\lambda}_1^{\mathrm{T}},$ such that the dissipation function reads $\mathsf{D}(\boldsymbol{d}^{\mathrm{p}})=\boldsymbol{\sigma}:\boldsymbol{d}^{\mathrm{p}}=\varphi(\boldsymbol{\sigma})\psi(\boldsymbol{d}^{\mathrm{p}})=\sigma_1^{\mathrm{T}}\dot{\lambda}_1^{\mathrm{T}},$ where the scalar $\dot{\lambda}_1^{\mathrm{T}}$ is the equivalent plastic strain rate associated with the adopted equivalent stress measure, i.e. the uniaxial tensile stress, $\boldsymbol{\sigma}$ is the Cauchy stress tensor and $\boldsymbol{d}^{\mathrm{p}}$ its work-conjugate, i.e., the Eulerian plastic strain-rate tensor.

The approximate[1] macroscopic SRP, $\Psi(\boldsymbol{D}),$ associated with the imposed macroscopic strain rate tensor, $\boldsymbol{D}=\langle\boldsymbol{d}\rangle_\Omega$, and the Rice and Tracey [5] microscale trial strain-rate field, $\boldsymbol{d}^{\mathrm{RT}}(\underline{\boldsymbol{x}})=\boldsymbol{D}'+D_{\mathrm{m}}(b/r)^3(-2\underline{\boldsymbol{e}}_r\otimes\underline{\boldsymbol{e}}_r+\underline{\boldsymbol{e}}_\theta\otimes\underline{\boldsymbol{e}}_\theta+\underline{\boldsymbol{e}}_\phi\otimes\underline{\boldsymbol{e}}_\phi),$ (where $\boldsymbol{D}'$ and D_{m} represent the deviatoric and the hydrostatic part of $\boldsymbol{D}$, and $(\underline{\boldsymbol{e}}_r,\underline{\boldsymbol{e}}_\theta,\underline{\boldsymbol{e}}_\phi)$ is the orthonormal base of the spherical (r,θ,ϕ) coordinate system), is defined as:

$$\Psi(\boldsymbol{D})=(1-f)\left\langle\psi\left(\boldsymbol{d}^{\mathrm{RT}}\right)\right\rangle_{\Omega\setminus\omega}=\frac{1}{V}\int_A^B A(r)\left\langle\psi\left(\boldsymbol{d}^{\mathrm{RT}}\right)\right\rangle_{S(r)}dr, \tag{4}$$

where the notations $\langle\cdot\rangle_V$ and $\langle\cdot\rangle_{S(r)}$ stand for volume averaging over the volume V, and over the surface $S(r)=\{\underline{\boldsymbol{x}}\in\mathbb{R}^3:\|\underline{\boldsymbol{x}}\|_2=r\},$ respectively, with $S(r)$ denoting the spherical surface of radius r and area $A(r)=4\pi r^2.$ The above integral is determined numerically by the cubature procedure proposed in Brito [3]. Moreover, one can define its dual, the macroscopic stress potential, $\Phi(\boldsymbol{\Sigma}),$ by applying the normality principle at the macroscale:

$$\boldsymbol{D}=\dot{\Lambda}\frac{\partial\Phi}{\partial\boldsymbol{\Sigma}}(\boldsymbol{\Sigma})\Leftrightarrow\begin{cases}\dfrac{\boldsymbol{\Sigma}}{\sigma_1^{\mathrm{T}}}=\dfrac{\partial\Psi(\boldsymbol{D})}{\partial\boldsymbol{D}}\\ \Psi(\boldsymbol{D})=\dot{\Lambda}\end{cases},\ \dot{\Lambda}\geq 0, \tag{5}$$

where scalar $\dot{\Lambda}$ is the macroscopic plastic multiplier rate and $\boldsymbol{\Sigma}$ is the macroscopic Cauchy stress. The criterion in Eq. 4 is implemented in an academic FE research code (DD3IMP, University of Coimbra, e.g. [7]–[9]) considering a large-strain elastoplastic constitutive framework grounded on an hyperelastic-based elastic-plastic multiplicative split formulation and based on the strain-rate potential flow rule (i.e. right member of Eq. 5) to describe the plastic dissipation (see also [3] for details). Given the adopted numerical approach to the homogenization problem, the model presented above is coined the Computational Homogenization Model (CHM).

[1] Approximate in the sense that a *single* trial velocity field, $\boldsymbol{d}^{\mathrm{tr}}=\boldsymbol{d}^{\mathrm{tr}}(\underline{\boldsymbol{x}},\boldsymbol{D}),\ \forall\underline{\boldsymbol{x}}\in\Omega\setminus\omega,$ compatible with uniform strain-rate boundary conditions of the type $\underline{\boldsymbol{v}}(\underline{\boldsymbol{x}}=B\underline{\boldsymbol{e}}_r)=\boldsymbol{D}\underline{\boldsymbol{x}},$ is employed, where $\underline{\boldsymbol{x}}$ is the position vector in the Representative Volume Element and $\Omega\setminus\omega$ denotes the domain of the matrix phase.

Materials Research Proceedings 41 (2024) 1231-1239 https://doi.org/10.21741/9781644903131-137

Finite element model

The finite element (FE) simulation of the cup-drawing test is based on the work of Yoon et al. [4]. Both the process parameters and the constitutive identification of the yield behaviour of the AA5042-H2 matrix are extracted from the cited paper. A schematic view of the cylindrical cup drawing setup is shown in Fig. 1. The process parameters and the dimensions of the tools are given in Table 1. Given the geometric and orthotropic symmetry conditions of the cup drawing process, the analysis is confined to one quarter of the model. The adopted FE mesh is shown in Fig. 2. The structured zone is discretized with a 30×28 (radial × circumferential) partition in the plane of the sheet and two layers along the thickness direction are used. The FE mesh consists of a total of 1896 eight-node hexahedral FE with a selective reduced integration (SRI) technique. The tools are modelled as rigid bodies and the friction between the sheet and the tools is assumed constant and characterized by Coulomb's law with a friction coefficient $\mu = 0.008$ (after [4]).

The matrix plastic behaviour is caracterized with the non-quadratic form of CPB06ex2 [2] yield criterion (i.e. using two ortotropic transformations); and its elastic behaviour is assumed isotropic and constant, as the degradation of the elastic modulus is neglected. The isotropic hardening of the matrix is described by a Voce-type law: $Y_{\mathrm{Voce}}(\bar{\varepsilon}_{\mathrm{M}}^{\mathrm{p}}) = Y_0 + (Y_{\mathrm{sat}} - Y_0)(1 - e^{-C_{\mathrm{Y}}\bar{\varepsilon}_{\mathrm{M}}^{\mathrm{p}}})$, where Y_{Voce} is the yield stress, $\bar{\varepsilon}_{\mathrm{M}}^{\mathrm{p}}$ is the matrix equivalent plastic strain and $\{Y_0, Y_{\mathrm{sat}}, C_{\mathrm{Y}}\}$ are the Voce parameters. Strain-controlled nucleation is considered via Chu and Needleman's [10] normal distribution, yet stress-controlled nucleation is neglected. Table 2 summarizes the material model parameters.

Fig. 3 represents cross sections of the macroscopic SRP (Eq. 4) and the respective conjugate, the macroscopic yield surface, in the principal space with varying hydrostatic levels. Note that the shape of the sections changes drastically along the hydrostatic axis. Initially departing from a shape reminiscent to that of the dense phase, the sections progressively evolve towards a more smooth, rounded form (i.e. approaching isotropy) near the poles. Closed-form analytical criteria for porous solids are unable to capture such evolving shape behaviour as the underlying shape in the purely deviatoric plane is maintained throughout the hydrostatic axis. Moreover, it is worth noting that the positions of the extreme hydrostatic values are not on the hydrostatic axis. This is a result of the anisotropy alone (indeed, tension-compression asymmetry is assumed null for this matrix alloy) and renders the potentials remarkably asymmetrical with respect to the purely deviatoric plane (these are, however, symmetric with respect to the origin, since tension-compression asymmetry is neglected and thus the governing microscale criteria are even functions).

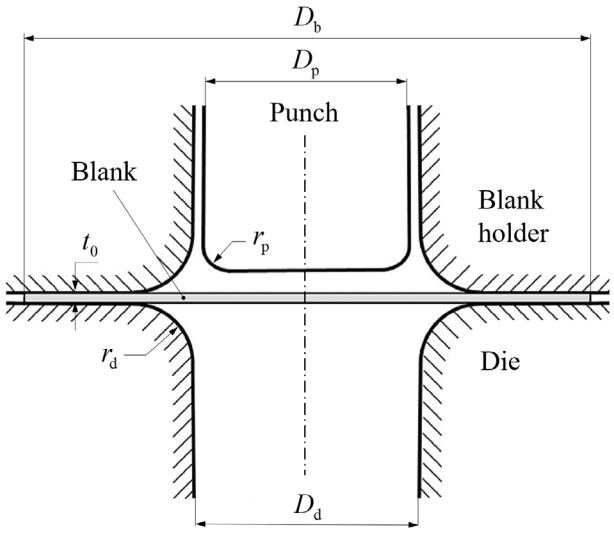

Figure 1. Schematic representation of a cylindrical cup drawing process (adapted from [11]).

Table 1. Process parameters and the dimensions of the tools (after [4]).

Parameter		Value	
Blank diameter	D_b	76.07	[mm]
Die opening diameter	D_d	46.74	[mm]
Punch diameter	D_p	45.72	[mm]
Die profile radius	r_d	2.28	[mm]
Punch profile radius	r_p	2.28	[mm]
Initial blank thickness	t_0	0.274	[mm]
Punch stroke	u_p	22.75	[mm]
Blank-holder force (total)	f_{bh}	10.0	[kN]

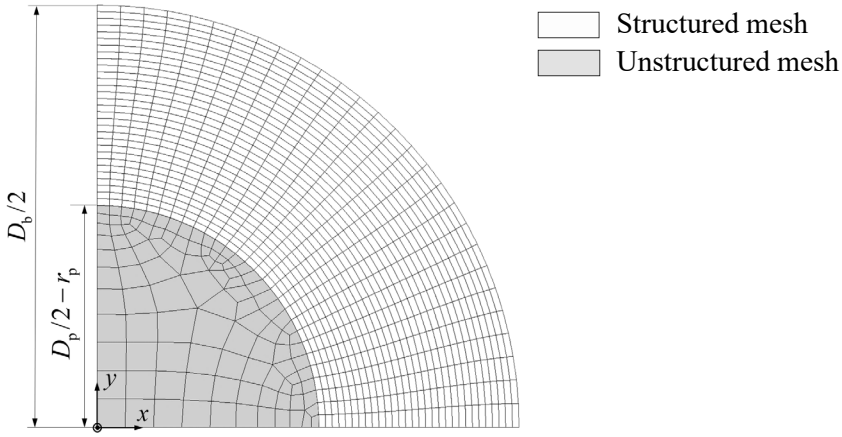

Figure 2. FE mesh of the blank in the reference configuration. Two through-thickness layers are used.

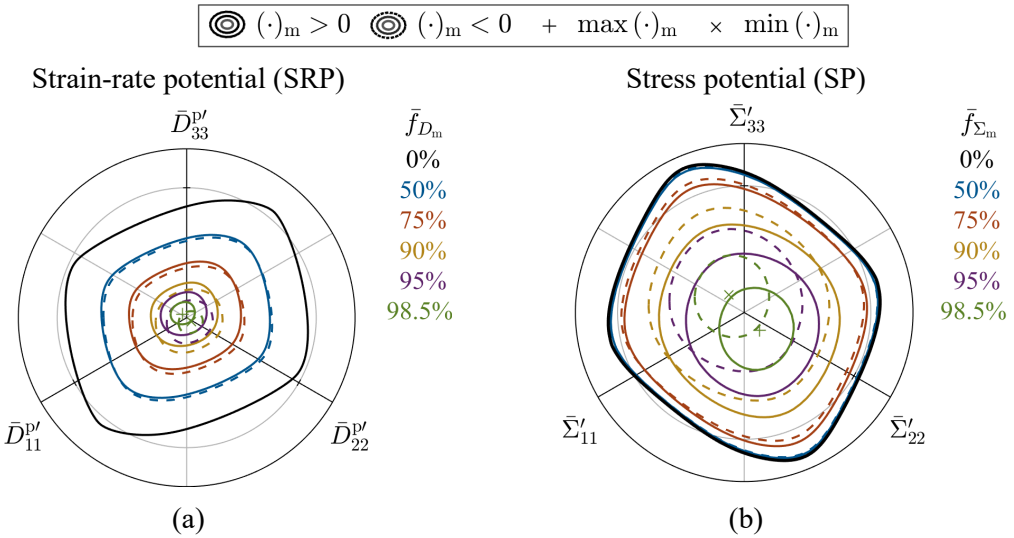

Figure 3. π-plane representation of macroscopic: (a) strain-rate potential (Eq. 4); and (b) stress potential; unitary isovalue surfaces in their respective principal space for a porous solid with porosity $f_0 = 0.001$, with a AA5042-H2 alloy matrix. Cross sections with varying hydrostatic fraction, $\bar{f}_{(\cdot)_m}$, with respect to the tensile and compressive hydrostatic extreme values are plotted.

Table 2. Material coefficients for the AA5042-H2 alloy (partially after [4]).

Elasticity (isotropic)									
Young modulus [GPa]	Poisson ratio [-]								
E	υ								
68.9	0.33								
Plasticity: *matrix behaviour*									
CPB06ex2 parameters ($a=10$)									
$k^{(1)}$	$C_{11}^{(1)}$	$C_{12}^{(1)}$	$C_{13}^{(1)}$	$C_{22}^{(1)}$	$C_{23}^{(1)}$	$C_{33}^{(1)}$	$C_{44}^{(1)}$	$C_{55}^{(1)}$	$C_{66}^{(1)}$
0.0	1.0	-0.0272	-0.6011	1.2870	0.6864	-0.2736	1.0	1.0	1.1514
$k^{(2)}$	$C_{11}^{(2)}$	$C_{12}^{(2)}$	$C_{13}^{(2)}$	$C_{22}^{(2)}$	$C_{23}^{(2)}$	$C_{33}^{(2)}$	$C_{44}^{(2)}$	$C_{55}^{(2)}$	$C_{66}^{(2)}$
0.0	1.0	-0.0897	0.0112	1.1322	-0.1092	-1.2009	1.0	1.0	1.3093
Isotropic hardening									
Voce law									
Y_0 [MPa]	Y_{sat} [MPa]	C_Y [-]							
267.80	375.08	17.859							
Porosity									
Initial porosity	Critical porosity	Strain-controlled nucleation							
f_0	f_C	f_N	$\bar{\varepsilon}_N$	s_N					
0.001	0.1	0.01	0.3	0.1					

Results and discussion

The simulation of the cup drawing test is performed for three SRP plasticity models: (i) the dense model (the dual of the CPB06ex2 criterion in Eq. 1); (ii) the Gurson [1] (isotropic) porous criterion; and (iii) the CHM described in Eq. 4. All simulations were executed on a computer equipped with an Intel® Core™ i7-8700K (6C/12T) CPU on a 64-bit Windows 10 Pro for Workstations operating system. Table 3 summarizes the computational performance of the numerical simulations for each material model. Fig. 4 depicts the predicted geometry of the completely drawn cup using the CHM. This model predicts the occurrence of eight ears of varying height, which agrees with experimental data, as shown in Fig 5. Fig. 5 also shows that a comparable earing height trend is captured using the CPB06ex2 (dense) criterion, yet, quantitatively, the latter model predicts higher earing profile. This is thought to result from the restrictive condition of plastic incompressibility in the CPB06ex2 model, which facilitates the elongation of the sheet in the blank holder zone.

Table 3. Computational performance measurements of the cup drawing test simulations for the three plasticity models: the dense model (CPB06ex2, Eq. 1); the Gurson (1977) model; and the computational homogenization model (CHM, Eq. 4)

		Dense	Gurson	CHM
No. of increments		129	121	124
Computational time	Absolute [h]	2.73	0.18	46.97
	Relative	1.0	0.066	20.42

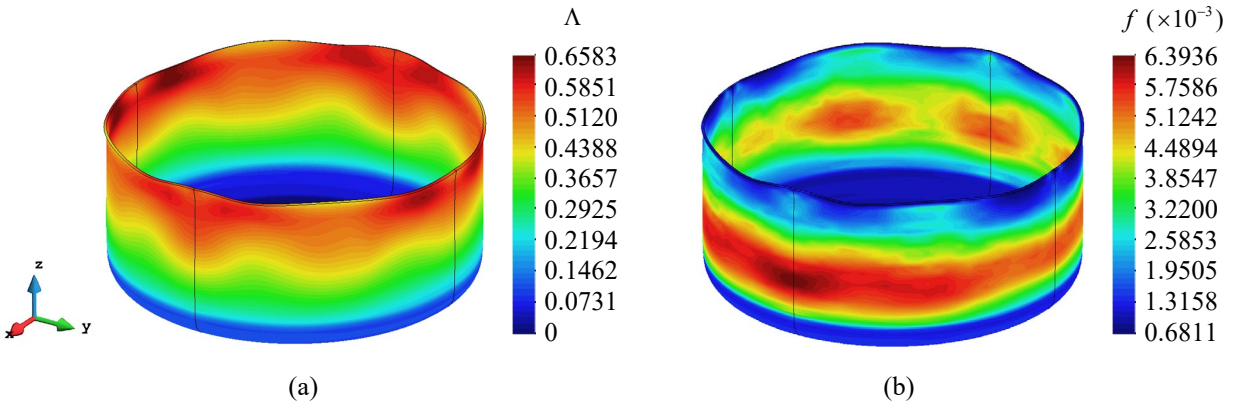

(a) (b)

Figure 4. Completely drawn cup. Isocontours of the: (a) accumulated equivalent plastic strain, $\Lambda = \int \dot{\Lambda} dt$; and (b) the porosity, f, using the computational homogenization model (CHM, Eq. 4).

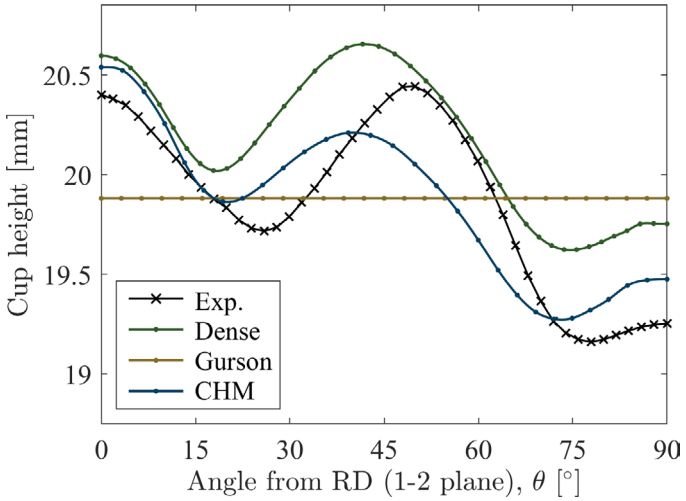

Figure 5. FE results of the earing profile of the completely drawn cup using: the dense model (CPB06ex2, Eq. 1); the Gurson (1977) model; and the computational homogenization model (CHM, Eq. 4). Comparison with experimental data (after [4]).

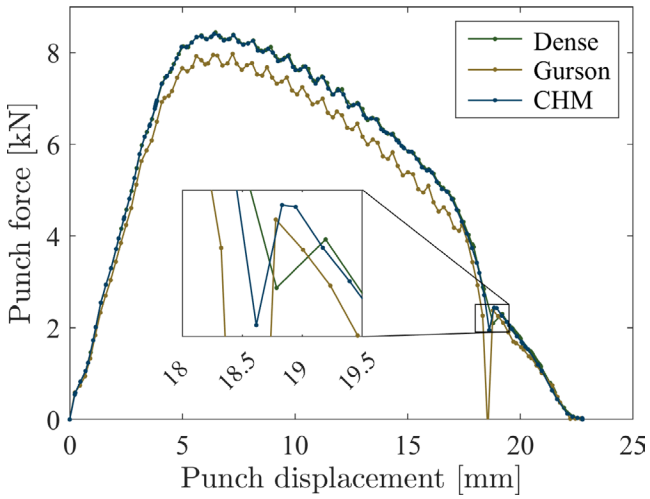

Figure 6. FE results of the punch force-displacement curves using: the dense model (CPB06ex2, Eq. 1); the Gurson (1977) model; and the computational homogenization model (CHM, Eq. 4).

The punch force-displacement evolution as predicted by each model is represented in Fig. 6, including the detail for the instance the blank lost contact with the blank-holder. The criteria that consider matrix orthotropy (CPB06ex2 and the CHM) predict virtually the same result, whereas

the curve associated with Gurson's isotropic model appears to be a lower bound estimate throughout the entire drawing process. Unfortunately, no experimental data is available to assess the quality of these predictions.

Conclusions

In this work, a numerical approach to the Gurson-type homogenization problem was employed to describe the damage state of a highly textured alloy whose orthotropy is modelled based on a non-quadratic yield function with multiple linear transformations. In contrast with existing closed-form *ad hoc* criteria, the employed formulation accounts for the micro-macro plasticity coupling as accurately as allowed by the scale transition operations (Hill-Mandel lemma and limit analysis theory). The primary drawback lies in the higher computational cost incurred with the utilization of cubature methods for the assessment of volume integrals. Nonetheless, it is shown that this cost is not prohibitively expensive. Moreover, a surge in the number of cores of new chips is due in next few years driven by the demands of emerging technologies such as artificial intelligence (AI) and virtual reality (VR), hence the heightened computational effort associated with the employed numerical homogenization scheme is expected to be mitigated by the rapid advancements in microprocessor performance and parallelism within a short timeframe.

References

[1] A. Gurson, "Continuum Theory of Ductile Rupture by Void Nucleation and Growth: Part I-Yield Criteria and Flow Rules for Porous Ductile Media," *J Eng Mater Technol*, vol. 99, no. 1, pp. 2–15, Jan. 1977. https://doi.org/10.1115/1.3443401

[2] B. Plunkett, O. Cazacu, and F. Barlat, "Orthotropic yield criteria for description of the anisotropy in tension and compression of sheet metals," *Int J Plast*, vol. 24, no. 5, pp. 847–866, 2008. https://doi.org/10.1016/j.ijplas.2007.07.013

[3] J. P. Brito, "Numerical-based plastic potentials for anisotropic porous metallic materials: development and implementation," PhD Thesis, University of Coimbra, 2023.

[4] J.-H. Yoon, O. Cazacu, J. W. Yoon, and R. E. Dick, "Earing predictions for strongly textured aluminum sheets," *Int J Mech Sci*, vol. 52, no. 12, pp. 1563–1578, 2010. https://doi.org/10.1016/j.ijmecsci.2010.07.005

[5] J. R. Rice and D. M. Tracey, "On the ductile enlargement of voids in triaxial stress fields," *J Mech Phys Solids*, vol. 17, no. 3, pp. 201–217, 1969. https://doi.org/10.1016/0022-5096(69)90033-7

[6] O. Cazacu, B. Plunkett, and F. Barlat, "Orthotropic yield criterion for hexagonal closed packed metals," *Int J Plast*, vol. 22, no. 7, pp. 1171–1194, 2006. https://doi.org/10.1016/j.ijplas.2005.06.001

[7] M. C. Oliveira, J. L. Alves, and L. F. Menezes, "Algorithms and strategies for treatment of large deformation frictional contact in the numerical simulation of deep drawing process," *Archives of Computational Methods in Engineering*, vol. 15, no. 2, pp. 113–162, 2008. https://doi.org/10.1007/s11831-008-9018-x

[8] L. F. Menezes and C. Teodosiu, "Three-dimensional numerical simulation of the deep-drawing process using solid finite elements," *J Mater Process Technol*, vol. 97, no. 1–3, pp. 100–106, 2000. https://doi.org/10.1016/S0924-0136(99)00345-3

[9] D. M. Neto, M. C. Oliveira, L. F. Menezes, and J. L. Alves, "Applying Nagata patches to smooth discretized surfaces used in 3D frictional contact problems," *Comput Methods Appl Mech Eng*, vol. 271, pp. 296–320, 2014. https://doi.org/10.1016/j.cma.2013.12.008

[10] C. C. Chu and A. Needleman, "Void Nucleation Effects in Biaxially Stretched Sheets," *J Eng Mater Technol*, vol. 102, no. 3, pp. 249–256, Jul. 1980. https://doi.org/10.1115/1.3224807

[11] J.-W. Yoon, F. Barlat, R. E. Dick, K. Chung, and T. J. Kang, "Plane stress yield function for aluminum alloy sheets-part II: FE formulation and its implementation," *Int J Plast*, vol. 20, no. 3, pp. 495–522, 2004. https://doi.org/10.1016/S0749-6419(03)00099-8